Multi-user Detection Techniques using Maximum Likelihood Sphere Decoding in Multi-Carrier CDMA Systems*

Loïc BRUNEL

Mitsubishi Electric ITE, Telecommunication Laboratory
1, allée de Beaulieu, CS 10806, 35708 Rennes Cedex 7, France
brunel@tcl.ite.mee.com

July, 2002
Revised December, 2002

Abstract

When performed using an exhaustive search, the maximum likelihood (ML) joint detection of all users in a multi-carrier code division multiple access (MC-CDMA) system has a prohibitive complexity, growing exponentially with the number of users and the number of bits in each modulation symbol. In this paper, a novel ML multiuser detection algorithm is proposed, the complexity of which is a polynomial function of the number of users and is independent of the modulation size. The MC-CDMA system is modelled as a sphere packing lattice and a low-complexity optimum lattice decoder, the sphere decoder, is applied to jointly detect all users. Sub-optimum simplifications, based on the orthogonal projection of the received signal on a facet of the lattice constellation, are also proposed to further decrease the complexity. Simulation results are shown with up to 64 users transmitting 16-QAM symbols.

Key Words: Lattice Decoding, Multi-Carrier CDMA, Multiuser Detection.

*Part of the material in this paper has been presented in the 12th IEEE Int. Symp. on Personal, Indoor and Mobile Radio Communications (PIMRC'01), San Diego, USA, Sept. 2001, and in the IEEE Int. Conf. on Communications (ICC'02), New York, USA, Apr. 2002. The basis vector reordering presented in section 4.2 has been studied in the framework of the IST-2001-32620 MATRICE project.

1 Introduction

The multi-carrier code division multiple access (MC-CDMA) technique, initially proposed by [3][6][16], efficiently combines the orthogonal frequency division multiplex (OFDM) modulation and the code division multiple access technique. In direct sequence code division multiple access (DS-CDMA), the signature and the signal of each user are multiplied in the time domain, whereas, in MC-CDMA, the signature and the signal are multiplied in the frequency domain. Each user symbol is transmitted over several sub-carriers. On each sub-carrier, this signal is multiplied by a distinct element of a user-specific signature. In other words, the transmitted symbol is spread before OFDM modulation. Low cross-correlation values between signatures are desirable to enable user separation at the receiver. Thanks to the guard interval between OFDM symbols, MC-CDMA systems do not suffer from inter-symbol interference (ISI) and quasi-synchronism between users may be obtained in the uplink. Furthermore, the OFDM modulation takes advantage of a large frequency diversity. To combat the multiuser interference due to the loss of orthogonality introduced by the transmission on a multipath channel, various single-user and multiuser detection techniques have been proposed [9]. Among them, the optimum multiuser detection, based on a maximum likelihood (ML) exhaustive search [6], has a prohibitive complexity, growing exponentially with the number of users and the number of bits per modulation symbol.

We propose a new optimum detection algorithm with low complexity for MC-CDMA systems. This algorithm, called the sphere decoding algorithm, originally employed for sphere packing lattice decoding [14][15], has recently been proposed to simplify the ML multiuser detection in DS-CDMA [1][2]. In MC-CDMA, the receiver models the maximum ratio combining (MRC) output as a multi-dimensional sphere packing lattice point corrupted by additive noise. The lattice sphere decoder is then applied to jointly detect all users. Its complexity is a polynomial function of the number of users and is independent of the modulation size. Thus, it allows optimum performance even for full-loaded

systems using large modulations. The absence of ISI and the synchronism assumption make the MC-CDMA a particularly suitable system for lattice representation and sphere decoding. However, for a large number of users, even with some simplifications like basis vector reordering, the decoding complexity may still be too high for very noisy received signals. In this case, we propose sub-optimum simplifications by orthogonal projection, which speed up the decoding process with low performance loss.

The paper is organised as follows: Section 2 describes the synchronous MC-CDMA system and the corresponding lattice representation. In section 3, the sphere decoding algorithm is detailed for lattice constellations and then applied to a MC-CDMA system in section 4. Simplifications introducing some sub-optimality are described in section 5. Simulation results for downlink are presented in section 6 and compared to the performance of classical sub-optimum detection algorithms. Finally, some conclusions are drawn in section 7.

2 Lattice Representation of a Synchronous MC-CDMA System

Let us represent a synchronous MC-CDMA system, or equivalently a quasi-synchronous MC-CDMA system without ISI, using a sphere-packing lattice [5]. A κ-dimensional sphere packing lattice of $\mathbb{R}^\nu$ is a discrete subgroup (or a $\mathbb{Z}$-module) with rank κ of $\mathbb{R}^\nu$. We denote $\mathbb{R}$ the real space and $\mathbb{Z}$ the integer ring. Each point $\mathbf{x}$ of lattice Λ may be written as the linear combination of κ basis row vectors $\mathbf{v}_k$:

$$\mathbf{x} = b_1\mathbf{v}_1 + \ldots + b_\kappa\mathbf{v}_\kappa \quad \text{where} \quad b_k \in \mathbb{Z}, \quad \forall k = 1, \ldots, \kappa. \tag{1}$$

Vectors $\mathbf{v}_k$ compose the $\kappa \times \nu$ lattice *generator matrix* $\mathbf{G}$. Thus, $\mathbf{x} = \mathbf{bG}$ where $\mathbf{b} = (b_1, \ldots, b_\kappa) \in \mathbb{Z}^\kappa$.

We consider a synchronous MC-CDMA system with K users as described in Fig. 1. At time i and for user k, the transmitted symbol $b_k(i)$, taken from a modulation alphabet $\mathcal{A}_k$

with cardinality $|\mathcal{A}_k|$, is spread by a signature $\mathbf{c} = (c_{k1}, \ldots, c_{kL})$, which has good cross-correlation properties with other user signatures. In this paper, signatures belong to an orthogonal Walsh-Hadamard set of size L. After spreading of $b_k(i)$, the L obtained chips are transmitted with signal amplitude ω_k on the L different sub-carriers of an OFDM modulation symbol. A guard interval Δ is inserted to absorb ISI. We denote $s_k(i)$ the modulated signal filtered by a frequency selective multipath channel. After addition of interfering user signals, $\sum_{k' \neq k} s_{k'}(t)$, and additive white Gaussian noise (AWGN), OFDM demodulation is performed. The channel is assumed non frequency selective on the sub-carrier bandwidth and is thus described by a single complex coefficient $h_{k\ell}(i)$ for each user k and each sub-carrier ℓ. We denote $\mathbf{C}(i)$ the $K \times L$ matrix merging spreading and channel coefficients for all users:

$$\mathbf{C}(i) = \begin{bmatrix} c_{11}h_{11}(i) & \cdots & c_{1L}h_{1L}(i) \\ \vdots & & \vdots \\ c_{K1}h_{K1}(i) & \cdots & c_{KL}h_{KL}(i) \end{bmatrix}. \tag{2}$$

At time i, the received vector $\mathbf{r}(i) = (r_1(i), \ldots, r_L(i))$ may be expressed as

$$\mathbf{r}(i) = \mathbf{b}(i)\mathbf{D}_\omega\mathbf{C}(i) + \boldsymbol{\eta}(i) \tag{3}$$

where vector $\mathbf{b}(i) = (b_1(i), \ldots, b_K(i))$ contains the K transmitted symbols, diagonal matrix $\mathbf{D}_\omega = \mathrm{diag}(\omega_1, \ldots, \omega_K)$ contains the user amplitudes and $\boldsymbol{\eta}(i) = (\eta_1(i), \ldots, \eta_L(i))$ is the AWGN vector. In downlink, all users share the same channel, defined by $\mathbf{H}(i) = \mathrm{diag}(h_1(i), \ldots, h_L(i))$. Thus, $\mathbf{C}(i) = \mathbf{C}_D\mathbf{H}(i)$, where all user signatures are placed in the $K \times L$ matrix $\mathbf{C}_D = \left(\mathbf{c}_1^T, \ldots, \mathbf{c}_K^T\right)^T$. Let us now consider the ML multiuser detection using the received signal given in expression (3). In order to maximise the likelihood of the received signal assuming the transmitted signal $\mathbf{b}$, since the noise $\boldsymbol{\eta}(i)$ is AWGN, we have to minimise the quadratic distance $d_{\mathrm{E}}^2(\mathbf{b})$ between the received signal and the signal expected to be received if $\mathbf{b}$ has been transmitted:

$$d_{\mathrm{E}}^2(\mathbf{b}) = \|\mathbf{r}(i) - \mathbf{b}\mathbf{D}_\omega\mathbf{C}(i)\|^2. \tag{4}$$

Equivalently, we may minimise

$$d^2(\mathbf{b}) = \|\mathbf{b}\mathbf{D}_\omega\mathbf{C}(i)\|^2 - 2\mathrm{Re}\,\langle \mathbf{b}\mathbf{D}_\omega\mathbf{C}; \mathbf{r}(i)\rangle \tag{5}$$

where the scalar product is

$$\begin{aligned}\langle \mathbf{b}\mathbf{D}_\omega\mathbf{C}; \mathbf{r}(i)\rangle &= \sum_{k=1}^{K} \omega_k b_k^* \sum_{\ell=1}^{L} c_{k\ell}^*(i) h_{k\ell}^*(i) r_\ell(i) \\ &\triangleq \sum_{k=1}^{K} \omega_k b_k^* y_k(i). \end{aligned} \tag{6}$$

$y_k(i)$ is the MRC output for user k [16]. Vector $\mathbf{y}(i) = (y_1(i), \ldots, y_K(i))$ is a sufficient statistic for the ML detection of transmitted vector $\mathbf{b}(i)$. The observation $\mathbf{y}(i)$ may be written in a matrix form from (6):

$$\mathbf{y}(i) \triangleq \mathbf{r}(i)\mathbf{C}^H(i) \tag{7}$$

where $.^H$ denotes the transpose-conjugate. By including expression (3) in expression (7), we obtain $\mathbf{y}(i)$ as a function of the transmitted vector $\mathbf{b}(i)$:

$$\mathbf{y}(i) = \mathbf{b}(i)\mathbf{D}_\omega\mathbf{C}(i)\mathbf{C}^H(i) + \mathbf{n}(i) = \mathbf{b}(i)\mathbf{M}(i) + \mathbf{n}(i) \tag{8}$$

where noise $\mathbf{n}(i) = (n_1(i), \ldots, n_K(i)) = \boldsymbol{\eta}(i)\mathbf{C}^H(i)$.

We now write all previously defined complex vectors (resp. matrices) with size K (resp. $K \times K$) as real vectors (resp. matrices) with size $2K$ (resp. $2K \times 2K$), e.g.,

$$\begin{aligned}\mathbf{b}_2(i) &= \left(b_1^R(i), b_1^I(i), \ldots, b_K^R(i), b_K^I(i)\right) \\ \mathbf{D}_{\omega,2} &= \mathrm{diag}\,(\omega_1, \omega_1, \ldots, \omega_K, \omega_K) \\ \mathbf{R}_2(i) &= \begin{bmatrix} R_{11}^R & R_{11}^I & \cdots & R_{1K}^R & R_{1K}^I \\ -R_{11}^I & R_{11}^R & \cdots & -R_{1K}^I & R_{1K}^R \\ \vdots & \vdots & & \vdots & \vdots \\ R_{K1}^R & R_{K1}^I & \cdots & R_{KK}^R & R_{KK}^I \\ -R_{K1}^I & R_{K1}^R & \cdots & -R_{KK}^I & R_{KK}^R \end{bmatrix} \end{aligned} \tag{9}$$

where elements of $\mathbf{R}(i) = \mathbf{C}(i)\mathbf{C}^H(i)$ are denoted R_{ij} and each complex value a is expressed as $a = a^R + j.a^I$. With the above notations, we obtain

$$\mathbf{y}_2(i) = \mathbf{b}_2(i)\mathbf{M}_2(i) + \mathbf{n}_2(i) \quad \text{with} \quad \mathbf{b}_2(i) \in \mathbb{Z}^{2K}. \tag{10}$$

$\mathbf{y}_2(i)$ is a point of a lattice Λ_2 in $\mathbb{R}^{2K}$, with dimension $2K$ and generator matrix $\mathbf{M}_2(i) = \mathbf{D}_{\omega,2}\mathbf{R}_2(i)$, corrupted by an additive noise $\mathbf{n}_2(i)$ with covariance matrix $N_0\mathbf{R}_2(i)$.

If symbols $b_k(i)$ belong to a quadrature amplitude modulation (QAM) with size M^2, $b_k(i) = (b_k^R(i), b_k^I(i)) \in (-M+1, -M+3, \ldots, M-3, M-1)^2$. In this case, to perfectly match the definition of a real lattice, where transmitted symbols belong to a segment of $\mathbb{Z}$, we apply the following transformation

$$\begin{aligned} \mathbf{y}'_2(i) &= \frac{1}{2}\left(\mathbf{y}_2(i) + (M-1, \ldots, M-1)\,\mathbf{M}_2(i)\right) \\ &= \mathbf{b}'_2(i)\mathbf{M}_2(i) + \mathbf{n}'_2(i) \end{aligned} \tag{11}$$

where

$$\mathbf{b}'_2(i) = \frac{1}{2}\left(\mathbf{b}_2(i) + (M-1, \ldots, M-1)\right) \in (0, 1, \ldots, M-1)^{2K}. \tag{12}$$

For other modulations, an appropriately chosen transformation must be applied to obtain integer coordinates. $\mathbf{y}'_2(i)$ is a point of a lattice Λ_2, with dimension $2K$ and generator matrix $\mathbf{M}_2(i)$, corrupted by an additive noise $\mathbf{n}'_2(i) = \mathbf{n}_2(i)/2$ with covariance matrix $\mathbf{R}_2(i)N_0/4$. If signatures are independent and all amplitudes are greater than zero, Λ_2 is a $\mathbb{Z}$-module with rank $2K$ of the $2K$-dimensional real space $\mathbb{R}^{2K}$. The multiple access system generates a point $\mathbf{b}'_2(i)\mathbf{M}_2(i)$ belonging to a constellation, i.e., a finite subset of lattice Λ_2, with size $|\mathcal{A}_1| \times \cdots \times |\mathcal{A}_K|$.

The MC-CDMA system is convenient for lattice representation since it does not experience ISI, thanks to the guard interval, and the frequency selectivity is easily taken into account. However, it requires the revaluation of the generator matrix each time the channel is modified. Using the lattice representation allows us to apply the sphere decoding algorithm [14][15], a low complexity ML decoding algorithm. This algorithm is directly inspired by an algorithm, which, for a given point in the space, finds the closest point

in the lattice (*closest vector problem*) [7]. Since the sphere decoding has a complexity in $\mathcal{O}(\kappa^6)$ [7] and since the lattice dimension for a complex modulation is twice the lattice dimension for a real modulation, the decoding complexity is 32 times higher per dimension with a complex modulation. The problem is simpler in the special case of a downlink transmission with real spreading, when the in-phase and quadrature signals are spread by the same real sequence, i.e., when matrix $\mathbf{C}_D$ is real valued:

$$\mathbf{M}(i) = \mathbf{D}_\omega \mathbf{C}_D \mathbf{H}(i) \mathbf{H}^H(i) \mathbf{C}_D^H = \mathbf{D}_\omega \mathbf{C}_D |\mathbf{H}(i)|^2 \mathbf{C}_D^T \tag{13}$$

where $|\mathbf{H}(i)|^2 = \text{diag}(|h_1(i)|^2, \ldots, |h_L(i)|^2)$ is a real matrix. Hence, matrix $\mathbf{M}(i)$ is real valued and the system may be modelled using a real lattice with dimension K and generator matrix $\mathbf{M}(i)$:

$$\begin{aligned} \mathbf{y}^R(i) &= \mathbf{b}^R(i)\mathbf{M}(i) + \mathbf{n}^R(i) \\ \mathbf{y}^I(i) &= \mathbf{b}^I(i)\mathbf{M}(i) + \mathbf{n}^I(i) \end{aligned} \tag{14}$$

where $\mathbf{y}^R(i)$, $\mathbf{b}^R(i)$ and $\mathbf{n}^R(i)$ (resp. $\mathbf{y}^I(i)$, $\mathbf{b}^I(i)$ and $\mathbf{n}^I(i)$) are vectors containing real parts (resp. imaginary parts) of the $\mathbf{y}(i)$, $\mathbf{b}(i)$ and $\mathbf{n}(i)$ elements. Noise vectors $\mathbf{n}^R(i)$ and $\mathbf{n}^I(i)$ have for covariance matrix $\mathbf{R}(i)N_0 = \mathbf{C}_D|\mathbf{H}(i)|^2\mathbf{C}_D^T N_0$. Such a representation for real spreading in downlink does not increase the decoding complexity per dimension when using a complex modulation symbol instead of a real one.

3 Sphere Decoding of a Lattice Corrupted by White Gaussian Noise

Let us first describe the ML decoding on AWGN channel of a κ-dimensional lattice Λ in $\mathbb{R}^\kappa$ generated by a real $\kappa \times \kappa$ matrix $\mathbf{G}$. The decoder has to find the closest lattice point to the received vector, i.e., the point which minimises the following metric:

$$m(\mathbf{y}|\mathbf{x}) = \sum_{k=1}^{\kappa} |y_k - x_k|^2 = \|\mathbf{y} - \mathbf{x}\|^2 \tag{15}$$

where $\mathbf{y} = \mathbf{x}+\boldsymbol{\eta}$ is the received vector, $\boldsymbol{\eta} = (\eta_1, \ldots, \eta_\kappa)$ the Gaussian noise vector and $\mathbf{x} = (x_1, \ldots, x_\kappa)$ a point of Λ. The noise vector $\boldsymbol{\eta}$ has real independent components with zero mean and variance N_0. Lattice points $\{\mathbf{x} = \mathbf{bG}\}$ are obtained from the data vectors $\mathbf{b} = (b_1, \ldots, b_\kappa) \in \mathbb{Z}^\kappa$.

In practice, the set of data vectors is limited to an alphabet $\mathcal{A}^{(\kappa)} \subset \mathbb{Z}^\kappa$ and an exhaustive ML decoder looks for the best point $\mathbf{x}$ among all points in the finite constellation. The sphere decoder restricts its computation to the points located inside a hypersphere with radius $\sqrt{C}$ centred on the received point, as shown on Fig. 2 for $\kappa = 2$ and a constellation with 20 points. Only lattice points located within the squared distance C from the received point are thus taken into account for the metric minimisation (15). The decoder performs the following minimisation:

$$\min_{\mathbf{x}\in\Lambda} \|\mathbf{y} - \mathbf{x}\| = \min_{\mathbf{w}\in\mathbf{y}-\Lambda} \|\mathbf{w}\|. \tag{16}$$

The above equality shows that the shortest vector $\mathbf{w}$ in the translated set $\mathbf{y} - \Lambda$ must be found. The difference $\mathbf{w} = \boldsymbol{\xi}\mathbf{G}$, $\boldsymbol{\xi} = (\xi_1, \ldots, \xi_\kappa) \in \mathbb{R}^\kappa$, is a lattice point, the coordinates of which are expressed on the translated basis centred on the received point $\mathbf{y} = \boldsymbol{\rho}\mathbf{G}$, $\boldsymbol{\rho} = (\rho_1, \ldots, \rho_K) \in \mathbb{R}^\kappa$. Since $\mathbf{x}$ must be located in a hypersphere with quadratic radius C centred on $\mathbf{y}$, $\mathbf{w}$ must be located in a hypersphere with same radius centred on $\mathbf{0}$:

$$\|\mathbf{w}\|^2 = \boldsymbol{\xi}\mathbf{G}\mathbf{G}^T\boldsymbol{\xi}^T \leq C. \tag{17}$$

In the new coordinates' system defined by $\boldsymbol{\xi}$, the hypersphere centred on $\mathbf{y}$ is changed into a hyperellipse centred on the origin. The Cholesky factorisation [4] of the Gram matrix $\boldsymbol{\Gamma} = \mathbf{G}\mathbf{G}^T$ yields $\boldsymbol{\Gamma} = \mathbf{A}\mathbf{A}^T$, where lower triangular matrix $\mathbf{A}$ has elements a_{ij}. Using (17), it can be shown [14][15], that a lattice point is inside the hypersphere if and only if

$$\forall k = 1, \ldots, \kappa, \quad B_{\min,k} \leq b_k \leq B_{\max,k}$$

$$\text{where} \quad B_{\min,k} = \left\lceil -\sqrt{\frac{1}{q_{kk}}\left(C - \sum_{\ell=k+1}^{\kappa} q_{\ell\ell}\left(\xi_\ell + \sum_{j=\ell+1}^{\kappa} q_{j\ell}\xi_j\right)^2\right)} + \rho_k + \sum_{j=k+1}^{\kappa} q_{jk}\xi_j \right\rceil$$

$$B_{\max,k} = \left\lfloor \sqrt{\frac{1}{q_{kk}} \left(C - \sum_{\ell=k+1}^{\kappa} q_{\ell\ell} \left(\xi_\ell + \sum_{j=\ell+1}^{\kappa} q_{j\ell} \xi_j \right)^2 \right)} + \rho_k + \sum_{j=k+1}^{\kappa} q_{jk} \xi_j \right\rfloor \quad (18)$$

$q_{kk} = a_{kk}^2$ for $k = 1, \ldots, \kappa$ and $q_{kj} = a_{kj}/a_{kk}$ for $j = 1, \ldots, \kappa$, $k = j+1, \ldots, \kappa$. Function $\lceil x \rceil$ is the *ceil* function, representing the lowest integer value higher than x and $\lfloor x \rfloor$ is the *floor* function, representing the highest integer value lower than x. κ internal counters, one counter per dimension, starting from dimension κ, enumerate all values of vector $\mathbf{b}$ such that the lattice point $\mathbf{x} = \mathbf{bG}$ is located within the quadratic distance C from the received point. Lattice points located outside the considered hypersphere are never tested. Consequently, the decoding complexity does not depend on the lattice constellation size $|\mathcal{A}^{(\kappa)}|$. Furthermore, the search is drastically speeded up by updating $\sqrt{C}$ with the last computed Euclidean norm $\|\mathbf{w}\|$ before looking for another point in the hypersphere [2]. Finally, the selected point $\mathbf{x}$ is the point associated to the minimum $\|\mathbf{w}\|$. Since the number of points located in the decoding hypersphere increases with radius $\sqrt{C}$, it must be carefully chosen. A large value slows down the algorithm, whereas the hypersphere may be empty if C is too small. By choosing a search radius equal to the lattice covering radius depicted on Fig. 2, we ensure that the decoder will find at least one lattice point in the hypersphere [15]. However, this point does not necessarily belong to the finite constellation $\mathcal{A}^{(\kappa)}$. Thus, if all lattice points in the sphere do not belong to the constellation, the radius must be slightly increased and sphere decoding performed again.

The sphere decoding may be easily applied to non-integer coordinates by enumerating given real values of b_k in the segments defined in (18).

4 Sphere Decoding of a Synchronous MC-CDMA System

In order to jointly detect all users in a MC-CDMA system, the sphere decoding is applied to the corresponding $2K$-dimensional lattice, one time for each received point, i.e., for

K users. In case of real spreading in downlink, it is applied to the corresponding K-dimensional lattice, twice for each received point. Let us restrict our explanation to the first case, the extension to real spreading in downlink being obvious. To simplify notations, we assume in the following that the modulation symbols are integers:

$$\forall k = 1, \ldots, K, \quad \mathcal{A}_k = \{b_{\min,k}, b_{\min,k} + 1, \ldots, b_{\max,k} - 1, b_{\max,k}\}^2 \tag{19}$$

and thus avoid transformation (11).

4.1 Noise Whitening

The additive noise samples included in the system model equation (10) are correlated. The ML lattice decoder has to minimise the following metric:

$$m'\left(\mathbf{y}_2\left(i\right)|\mathbf{x}_2\left(i\right)\right) = \left(\mathbf{y}_2\left(i\right) - \mathbf{x}_2\left(i\right)\right)\mathbf{R}_2^{-1}\left(i\right)\left(\mathbf{y}_2\left(i\right) - \mathbf{x}_2\left(i\right)\right)^T. \tag{20}$$

The sphere decoder may be easily adapted to the above optimisation, which describes the ML decoding of a lattice with generator matrix $\mathbf{M}_2(i)$ corrupted by a coloured noise $\mathbf{n}_2(i)$. Nevertheless, we prefer whitening the noise [13] at the MRC bank output, in order to use the same decoding procedure as described in section 3. The Cholesky factorisation of the cross-correlation matrix $\mathbf{R}_2(i)$ yields $\mathbf{R}_2(i) = \mathbf{W}_2(i){\mathbf{W}_2}^T(i)$, where $\mathbf{W}_2(i)$ is a lower triangular matrix. The whitened observation is

$$\tilde{\mathbf{y}}_2(i) = \mathbf{y}_2(i){\mathbf{W}_2}^{T^{-1}}(i) = \mathbf{b}_2(i)\mathbf{M}_2(i){\mathbf{W}_2}^{T^{-1}}(i) + \tilde{\mathbf{n}}_2(i) \tag{21}$$

where $\mathrm{E}\left[\tilde{\mathbf{n}}_2^T(i)\tilde{\mathbf{n}}_2(i)\right] = N_0\mathbf{I}_{2K}$. Thus, (20) is changed into a metric similar to (15). Equation (21) shows that, after the whitening operation, the observation must be processed with the sphere decoder associated to a new lattice generated by matrix

$$\mathbf{G}_2(i) = \mathbf{M}_2(i){\mathbf{W}_2}^{T^{-1}}(i) = \mathbf{D}_\omega\mathbf{W}_2(i) \tag{22}$$

in order to finally obtain the detected vector $\hat{\mathbf{b}}_2(i)$ [2]. The complete multiuser receiver structure, following the OFDM demodulation, is depicted on Fig. 3.

4.2 Taking the Constellation Structure into Account

Since the number of points per dimension in the constellation corresponds to the number of modulation symbols in phase or quadrature, this number is constant for a given dimension, whatever the values of other coordinates. Thus, the integer coordinates define a hypercube and the lattice constellation is a parallelogram, as depicted on Fig. 2. This special structure of the transmitted constellation allows us to reduce the complexity of the optimum detection in two ways.

Firstly, to ensure that $\hat{\mathbf{b}}_2(i)$ belongs to the transmitted constellation, bounds in (18) must be appropriately restricted:

$$\begin{aligned} \forall k = 1, \ldots, 2K, \quad & B'_{\min,k} \leq b_{2,k}(i) \leq B'_{\max,k} \\ \text{where} \quad B'_{\min,k} &= \max\left(B_{\min,k}, b_{\min,\lceil k/2 \rceil}\right) \\ B'_{\max,k} &= \min\left(B_{\max,k}, b_{\max,\lceil k/2 \rceil}\right). \end{aligned} \tag{23}$$

These restricted bounds avoid considering lattice points located in the search sphere but not belonging to the constellation. This restriction, preserving the algorithm optimality, yields a complexity reduction, which is higher with smaller constellations. Thus, the obtained complexity is not independent of the constellation size anymore.

Moreover, the order in which the lattice dimensions are treated for decoding has also a strong impact on the complexity. Let us consider the simple example depicted on Fig. 4, for which the lattice has dimension 2 ($K = 1$) and the constellation contains 16-QAM points ($b_{\min,1} = 0$, $b_{\max,1} = 3$). The received point is characterised in $\mathbb{Z}^2$ by its real coordinates $\boldsymbol{\rho}_2(i) = (\rho_{2,1}(i), \rho_{2,2}(i))$. All lattice points belonging to the constellation are represented by circles, coloured in grey if they are located in the hyperellipse and coloured in black otherwise. Grey crosses depict the lattice points located in the hyperellipse but not belonging to the constellation. Bounds are computed in (18) to cover all points in the hyperellipse and are then refined to take into account the constellation structure according to (23). On Fig. 5, the enumeration of all points in the hyperellipse is represented by a search tree.

In case 1, where bounds on dimension 2 are first computed, we see that points in the ellipse correspond to $b_2 \in \{0, 1, 2, 3\}$. These values are inside the constellation, thus they are all valid according to (23). For each possible value of b_2, bounds for b_1 are computed. E.g., for $b_2 = 2$, from (18) or Fig. 4, we get $b_1 \in \{3, 4, 5\}$. However, values 4 and 5 are not valid constellation points. This is the reason why, on Fig. 5, they are coloured in grey, as well as four other boxes among the eight boxes in dimension 1. Among the four possible values in dimension 2, only two values (2 and 3) correspond to valid constellation points. The computations of bounds on b_2, for b_1 equal to 0 and 1, were useless. These useless computations strongly slow down the algorithm for high dimensions.

Let us now consider case 2, in which bounds on b_1 are computed first. Points in the hyperellipse are such that $b_1 \in \{3, 4, 5\}$, but the single value in the constellation is $b_1 = 3$, which then yields $b_2 \in \{2, 3\}$. In the latter case, we only have to compute a single search segment per dimension, a total of two segments instead of 5 segments in the first case. This reduced number of considered segments is due to the strong reduction of cases in the first step of the algorithm. As these reductions correspond to dead ends in the search tree, the later they appear, the higher the useless computing complexity is.

The number of values discarded in a given dimension k, when considering the constellation bounds, increases when $\rho_k(i)$ is far outside the limits or, to a smaller extent, when $\rho_k(i)$ is inside the constellation but near the limits. From (18), we saw that the first considered segment corresponds to dimension $2K$. Thus, we propose to reorder the row basis vectors in generator matrix $\mathbf{G}_2(i)$ in the following manner:

Reordering criterion: The rows of $\mathbf{G}_2(i)$ are classified in an order increasing with the normalised distance δ between $\rho_k(i)$ and the constellation centre:

$$\delta = \frac{\left| \rho_k(i) - \frac{1}{2} \left(b_{\max,\lceil k/2 \rceil} + b_{\min,\lceil k/2 \rceil} \right) \right|}{b_{\max,\lceil k/2 \rceil} - b_{\min,\lceil k/2 \rceil}}. \tag{24}$$

This permutation of basis vectors yields the same permutation in detected symbols. The inverse permutation has to be applied to the detected integer coordinates to obtain

the symbol transmitted by each user.

5 Simplifications by Orthogonal Projection

The simplifications proposed in the previous section have no impact on the sphere decoder optimality. However, very noisy received vectors are received far away from the constellation. Hence, to preserve optimality, we must choose a search radius much larger than the covering radius and the algorithm becomes very slow. To ensure realistic decoding speed for noisy symbols, we propose to orthogonaly project them on the lattice constellation. The sub-optimality introduced by projection is expected to have a small impact on performance as it acts on very noisy and thus unreliable symbols.

5.1 Selection of the projection sub-space

As mentioned in section 4.2, the integer coordinates define a hypercube and the lattice constellation is a parallelogram, as depicted on Fig. 6a and 6b respectively. Fig. 6 shows how the dimension of the affine projection sub-space depends on the received vector location. It is easier to transpose the problem from the lattice real space (Fig. 6b) into the integer coordinate space (Fig. 6a). Instead of projecting directly on the constellation facet, we prefer assigning the following extended bounds to each dimension k:

$$\begin{aligned} f_{\min,k} &= b_{\min,k} - \alpha_k \\ f_{\max,k} &= b_{\max,k} + \alpha_k \end{aligned} \tag{25}$$

where α_k is a real positive value.

As depicted on Fig. 6, we use vector $\boldsymbol{\rho}_2(i) = \tilde{\mathbf{y}}_2(i)\mathbf{G}_2^{-1}(i)$ to determine on which affine sub-space we project the received point. Indeed, this vector shows us the received point's position with respect to the constellation and the type of projection we have to carry out: projection on a point for $\tilde{\mathbf{y}}_2(i)$ or projection on a straight line for $\tilde{\mathbf{y}}_2'(i)$. We choose the

following sub-optimum choice criterion:

Projection criterion 1: If Q dimensions are such that $\rho_{2,k}(i) \leq f_{\min,k}$ or $\rho_{2,k}(i) \geq f_{\max,k}$, we assign $f_{\min,k}$ or $f_{\max,k}$ to these values and we project on the corresponding affine sub-space $\mathcal{F}_N$ with dimension $N = 2K - Q$.

Fig. 7 shows how the projection, and even the projection choice, are sub-optimal. Only six points in the top-left angle of the constellation are represented. Decision bounds between some of these points are drawn in dashed lines. The two continuous lines are two projection affine sub-spaces. For the received vector $\tilde{\mathbf{y}}_2(i)$, the chosen projection is the best possible but the flat structure of the lattice gives rise to a detection error after projection: the optimum detection would select point A, whereas the sub-optimum version will detect point D. For the received vector $\tilde{\mathbf{y}}'_2(i)$, the chosen projection, in dashed line, is sub-optimal, the projection in continuous line would have been better. In this case, the sub-optimality of the projection leads to a detection error, since point D' is detected instead of point A'. Of course, this is not always the case, the chosen projection may not be optimal, whereas the detected point is correct.

5.2 Projection on the selected sub-space

Without loss of generality, we assume $\rho_{2,k}(i) \geq f_{\max,k}$, $k = 1, \ldots, Q$. Let $\mathbf{y}_2^P(i) = \boldsymbol{\rho}_2^P(i)\mathbf{G}_2(i)$ be the orthogonal projection of the whitened vector $\tilde{\mathbf{y}}_2(i)$ on the affine sub-space $\mathcal{F}_N$ with dimension N. According to projection criterion 1, the Q first coordinates are fixed to $f_{\max,k}$:

$$\rho_{2,k}^P(i) = f_{\max,k} \quad \text{for } k = 1, \ldots, Q. \tag{26}$$

Thus,

$$\mathbf{y}_2^P(i) = \boldsymbol{\rho}^0\mathbf{G}^0 + \boldsymbol{\rho}^1\mathbf{G}^1 = \mathbf{y}^0 + \boldsymbol{\rho}^1\mathbf{G}^1 \tag{27}$$

where $\boldsymbol{\rho}^0 = (f_{\max,1}, \ldots, f_{\max,Q})$ is a $1 \times Q$ row vector, $\mathbf{y}^0$ a $1 \times 2K$ row vector, $\boldsymbol{\rho}^1$ a $1 \times N$ row vector representing the degrees of freedom, $\mathbf{G}^0$ a $Q \times 2K$ matrix including the Q first

rows of $\mathbf{G}_2(i)$ and $\mathbf{G}^1$ a $N \times 2K$ matrix, including the N last rows of $\mathbf{G}_2(i)$ and building a basis of the vector sub-space $\mathcal{V}_N$. The projection on this vector sub-space, generated by rows of $\mathbf{G}^1$, can be easily written by

$$\mathbf{y}_2^P(i) = \left(\tilde{\mathbf{y}}_2(i) - \mathbf{y}^0\right).\mathbf{G}^{1\dagger}.\mathbf{G}^1 + \mathbf{y}^0 \tag{28}$$

where $\mathbf{G}^{1\dagger}$ is the pseudo-inverse of $\mathbf{G}^1$:

$$\mathbf{G}^{1\dagger} = \mathbf{G}^{1H}.\left(\mathbf{G}^1.\mathbf{G}^{1H}\right)^{-1}. \tag{29}$$

The projected point $\mathbf{y}_2^P(i)$ is closer to the constellation, hence the sphere detection in the $2K$-dimensional space will be faster. The gain in complexity will be all the higher as the signal to noise ratio will be small.

5.3 Sphere decoding in the reduced dimension lattice

Instead of considering the $2K$-dimensional lattice for sphere decoding, we may limit us to the N-dimensional lattice included in the projection sub-space $\mathcal{F}_N$. Indeed, points of lattice Λ_2 in $\mathbb{R}^{2K}$ contained in this N-dimensional affine sub-space are also points of a lattice Λ' in $\mathbb{R}^N$. If sphere decoding is performed on lattice Λ' with dimension $N \leq 2K$, the detection is further speeded up at the cost of a slight approximation: the detection simplification is based on the assumption that the transmitted point belongs to the facet on which the whitened vector $\tilde{\mathbf{y}}_2(i)$ has been projected, although the closest lattice point of Λ_2 might not belong to this facet. To proceed to the decoding in lattice Λ', the received point must be directly projected on the constellation facet:

Projection criterion 2: If Q dimensions are such that $\rho_{2,k}(i) \leq f_{\min,k}$ or $\rho_{2,k}(i) \geq f_{\max,k}$, the corresponding coordinates are fixed to $b_{\min,k}$ or $b_{\max,k}$.

Without loss of generality, we assume $\rho_{2,k}(i) \geq f_{\max,k}$, $k = 1, \ldots, Q$. According to projection criterion 2, the Q first coordinates are fixed to $b_{\max,k}$:

$$\rho_{2,k}^P(i) = b_{\max,k} \quad \text{for } k = 1, \ldots, Q. \tag{30}$$

From (21), we then write the projection as a point of Λ_2 corrupted with additive noise:

$$\mathbf{y}_2^P(i) = \mathbf{b}_2^P(i)\mathbf{G}_2(i) + \mathbf{n}_2^P(i) = \mathbf{b}^0\mathbf{G}^0 + \mathbf{b}^1\mathbf{G}^1 + \mathbf{n}_2^P(i) \tag{31}$$

where $\mathbf{b}^0 \in \mathbb{Z}^Q$, $\mathbf{b}^1 \in \mathbb{Z}^N$, $\mathbf{n}_2^P(i)$ is the noise vector. Since the transmitted point is assumed to belong to the projection facet, the Q first coordinates of the detected vector will be $\mathbf{b}^0 = (b_{\max,1}, \ldots, b_{\max,Q})$. Let us now focus on the detection of vector $\mathbf{y}^1$ with dimension $2K$ belonging to the vector sub-space $\mathcal{V}_N$ and obtained by subtracting the constant vector $\mathbf{y}^0 = \boldsymbol{\rho}^0\mathbf{G}^0 = \mathbf{b}^0\mathbf{G}^0$ from (31):

$$\mathbf{y}^1 = \mathbf{y}^P - \mathbf{y}^0 = \mathbf{b}^1\mathbf{G}^1 + \mathbf{n}_2^P(i). \tag{32}$$

Matrix $\mathbf{G}^1$ contains N basis vectors with size $2K$. Thus, $\mathbf{y}^1$ is a noisy point of a N-dimensional lattice in $\mathbb{R}^{2K}$. In order to be treated by the decoding as presented in section 3, the observation vector must be a noisy point of a N-dimensional lattice Λ' in $\mathbb{R}^N$. We have to find a $N \times N$ matrix $\mathbf{B}^1$ generating a lattice equivalent to the lattice generated by $\mathbf{G}^1$ in $\mathbb{R}^{2K}$. Equation (17) is the single relation employed in the sphere decoding and involving the lattice structure, through the Gram matrix of the generator matrix. In order that the lattice generated by $\mathbf{B}^1$ be equivalent to the lattice generated by $\mathbf{G}^1$, both matrices must have the same Gram matrix. Thus, $\mathbf{B}^1$ can be found by Cholesky factorisation of the Gram matrix of $\mathbf{G}^1$:

$$\mathbf{G}^1.\mathbf{G}^{1T} = \mathbf{B}^1.\mathbf{B}^{1T}. \tag{33}$$

Let $\mathbf{U}$ be the $2K \times N$ transfer matrix such that $\mathbf{B}^1 = \mathbf{G}^1\mathbf{U}$. It can be shown that

$$\mathbf{U} = \mathbf{G}^{1T}.\left(\mathbf{B}^{1^{-1}}\right)^T. \tag{34}$$

If row vector $\mathbf{x}^1 = \mathbf{b}^1\mathbf{G}^1$ is a point of the lattice in $\mathbb{R}^{2K}$, then vector $\mathbf{x}^{1'} = \mathbf{x}^1\mathbf{U} = \mathbf{b}^1\mathbf{B}^1$ with size N is a point of Λ'. Hence, the same transformation has to be performed on $\mathbf{y}^1$ before detection:

$$\mathbf{y}^{1'} = \mathbf{y}^1\mathbf{U} = \left(\mathbf{b}^1\mathbf{G}^1 + \mathbf{n}_2^P(i)\right)\mathbf{U} = \mathbf{b}^1\mathbf{B}^1 + \mathbf{n}^{1'}. \tag{35}$$

We can easily show that $E\left[\mathbf{n}^{1'T}\mathbf{n}^{1'}\right] = N_0\mathbf{I}_N$. No further noise whitening is necessary. Elements of $\mathbf{b}^1$, obtained by sphere decoding of vector $\mathbf{y}^{1'}$, are the non-fixed integer coordinates of the detected vector. Together with the fixed elements of $\mathbf{b}^0$, they form the detected vector $\hat{\mathbf{b}}_2$.

6 Simulation Results

The sphere decoding has been tested in downlink on an indoor channel defined in [12], with a delay spread equal to 390 ns. All users have the same power and transmit 16-QAM symbols on $L = 64$ sub-carriers over a 20 MHz bandwidth. With a HIPERLAN/2-like guard interval (25% of the OFDM symbol period), the obtained bit rate is 1 Mbit/s/user. Thus, with the 16-QAM high spectral efficiency, a total bit rate equal to 64 Mbit/s is reached for full-load. The channel coefficients change for each transmitted symbol. We assume the power control being perfect, i.e., at each time i, the received symbol power is equal to the transmitted symbol power.

In this section, three detection schemes with sphere decoding are tested. The sphere decoder A is the optimum one, whereas sphere decoders B and C include the projection described in section 5. Sphere decoding is performed in dimension $2K$ for scheme B and in reduced dimension N for scheme C. For both schemes, we chose $\alpha_k = 0$ for $k = 1, \ldots, 2K$.

On Fig. 8, for half-load (32 users), we compare the optimum performance of the sphere decoding with the performance of four sub-optimum detection schemes: the single-user minimum mean square error combining (MMSEC) [3], the multiuser parallel interference cancellation (PIC) with 2 iterations including MMSEC and hard cancellation [6], the multiuser global minimum mean square error (GMMSE) detector [10] and finally the multiuser decision-feedback minimum mean square error (DF-MMSE) detector inspired by its homonym in DS-CDMA [11]. The bit error rate (BER) averaged over all users is drawn versus the signal-to-noise ratio (SNR). The optimum multiuser performance is very close to the single-user one. The improvement with respect to DF-MMSE detection

is 1 dB for a BER equal to 10^{-3}. The gap with MMSEC, PIC and GMMSE detection schemes is even higher. Both B and C simplified versions of the sphere decoding have no impact on performance even with the chosen α_k values, which maximise the number of projections.

On Fig. 9, the required SNR to obtain an average BER equal to 10^{-3} is drawn versus the number of users. The gap in performance between optimum multiuser sphere decoder A and the single user bound increases with the system load. This degradation equals 2.7 dB for 64 users (full-load), whereas the degradation of DF-MMSE equals 7.5 dB. The performance loss due to the restriction of sphere decoder C to lattice Λ' is negligible with up to 56 users. Beyond this value, the performance degradation induced by the simplification sub-optimality grows sharply. Nevertheless, the sphere decoder C performance still remains better than the GMMSE and DF-MMSE performance, except for 64 users, but intermediate performance results, closer to the optimum sphere decoder A, may be obtained for sphere decoder C by increasing α_k values. The cost of this modification is obviously a complexity increase.

Table 1 illustrates the impact of basis vector reordering on the complexity of a system with 48 users and a SNR equal to 12 dB. The decoding complexity per user, averaged over a high number of detection operations, is divided by a factor greater than 25 when lattice basis vectors are reordered as proposed in section 4.2. It is worth reminding that this dramatic simplification does not impact on optimality.

Table 2 presents the averaged complexity per user of the proposed detectors with 56 users and a SNR equal to 12 dB. In all detectors, lattice basis vectors have been reordered. In sphere decoder C, complexity is reduced by a factor of 10 compared to the optimum sphere decoder A, by applying sub-optimum simplifications. The performance loss is negligible as shown by Fig. 9. Results for sphere decoder B are not presented, since its complexity is close to the one of sphere decoder A and its performance close to the one of sphere decoder C. In sphere decoders A' and C', a complexity control was applied to sphere decoders A and C. It means that the sphere decoding was stopped when the total

detection complexity of a point exceeded 10^9 operations. This coarse simplification divides the average complexity in sphere decoder A' by a factor 23, with a negligible performance loss. The complexity is further reduced by a factor of 1.4 when adding the projection to the complexity control, as done in sphere decoder C'. The final complexity is less than twice the complexity of a GMMSE or DF-MMSE detector. Finally, it is worth pointing out that, in such a system with 56 users and a 16-QAM modulation, an exhaustive ML search [6] would have required the computation of 2^{224} metrics to detect each vector $\mathbf{b}(i)$.

7 Conclusions

We studied and simplified a low complexity ML multiuser detection for MC-CDMA systems based on their lattice representation. This low complexity allows us to reach performance limits even for high loads and large modulations. The proposed simplifications further reduce the complexity. Although it was not tested for obvious simulation time reasons, the overall complexity gain in a 56-user system (87 % load) between the optimum sphere decoder without basis vector reordering and the sub-optimum sphere decoder with vector reordering, complexity control and projection, is expected to be far greater than 800, without performance loss. For higher loads, performance degradation appears, which, except for full-load, remains smaller than the one observed with DF-MMSE detector.

References

[1] L. Brunel, J. Boutros: "Euclidean space lattice decoding for joint detection in CDMA systems," *Proc. of ITW'99*, South Africa, p. 129, June 1999.

[2] L. Brunel, J. Boutros: "Lattice Decoding for Joint Detection in Direct Sequence CDMA Systems," *Accepted to IEEE Transactions on Information Theory*, May 2002, submitted Mar. 1999, revised Sept. 2000, Jan. 2002, *http://www.enst.fr/~brunel.*

[3] A. Chouly, A. Brajal, S. Jourdan: "Orthogonal multicarrier techniques applied to direct sequence spread spectrum CDMA systems," *Proc. of GLOBECOM'93*, pp. 1723-1728, Nov. 1993.

[4] H. Cohen: *Computational algebraic number theory*, Springer Verlag 1993.

[5] J.H. Conway, N.J. Sloane, *Sphere packings, lattices and groups*, 3rd ed., 1998, Springer-Verlag, New York.

[6] K. Fazel, L. Papke: "On the performance of convolutionally-coded CDMA/OFDM for mobile communication system," *Proc. of PIMRC'93*, pp. 468-472, Sept. 1993.

[7] U. Fincke, M. Pohst: "Improved methods for calculating vectors of short length in a lattice, including a complexity analysis," *Mathematics of Computation*, vol. 44, pp. 463-471, April 1985.

[8] G.D. Forney: "Coset codes I: introduction and geometrical classification," *IEEE Transactions on Information Theory*, vol. 34, pp. 1123–1151, 1988.

[9] S. Hara, R. Prasad: "Overview of multicarrier CDMA," *IEEE Communication Magazine*, pp. 126-133, Dec. 1997.

[10] J.F. Hélard, J.Y. Baudais, J. Citerne: "Linear MMSE detection technique for MC-CDMA," *Electronics Letters*, pp. 665-666, Mar. 2000.

[11] A. Klein, G.K. Kaleh, P.W. Baier: "Zero forcing and minimum mean-square-error equalization for multiuser detection in code-division multiple-access channels," *IEEE Transactions on Vehicular Technology*, vol. 45, pp. 276-287, May 1996.

[12] J. Medbo: "Channel models for HIPERLAN/2 in different indoor scenarios," *ETSI BRAN doc. 3ERI085b*, Mar. 1998.

[13] J.G. Proakis: *Digital communications, third edition*, McGraw-Hill, 1995.

[14] E. Viterbo and E. Biglieri: "A universal lattice decoder," *Proc. of 14ème Colloque GRETSI*, Juan-les-Pins, pp. 611-614, Sept 1993.

[15] E. Viterbo and J. Boutros: "A universal lattice code decoder for fading channels," *IEEE Transactions on Information Theory*, pp. 1639-1642, July 1999.

[16] N. Yee, J.P. Linnartz, G. Fettweis: "Multicarrier CDMA in indoor wireless radio networks," *Proc. of PIMRC'93*, Yokohama, pp. 109-113, Sept. 1993.

Author biography

Loïc Brunel (S'97-M'00) was born in Antony, France, in 1973. He received the electrical engineering degree and the Ph.D. degree of the Ecole Nationale Supérieure des Télécommuncations (ENST), Paris, France, in 1996 and 1999 respectively. Since January 2000, he has been a Research Engineer in the Telecommunication Laboratory of Mitsubishi Electric ITE in Rennes, France. His research interests are multi-carrier transmissions, code division multiple access, channel coding and antenna arrays.

List of Tables

List of Figures

Type of Sphere Decoder	Additions per user	Multiplications per user	Divisions per user	Others per user
Sphere Decoder A No basis vector reordering	5×10^5	5×10^5	4×10^4	4×10^4
Sphere Decoder A Basis vector reordering	2×10^4	2×10^4	9×10^2	7×10^2

Table 1: Impact on complexity of basis vector reordering (48 users, SNR = 11 dB, BER = 1.92×10^{-3}).

Type of Sphere Decoder	Additions per user	Multiplications per user	Divisions per user	Others per user	Average BER
Sphere Decoder A	3×10^5	3×10^5	2×10^4	2×10^4	1.47×10^{-3}
Sphere Decoder C	3.4×10^4	3.4×10^4	4.7×10^2	1.7×10^2	1.67×10^{-3}
Sphere Decoder A'	1.3×10^4	1.3×10^4	2.5×10^2	2.8	1.49×10^{-3}
Sphere Decoder C'	8.8×10^3	9.0×10^3	1.8×10^2	2.4	1.67×10^{-3}
GMMSE	5.2×10^3	5.3×10^3	2.8×10^1	0	8.51×10^{-3}
DF-MMSE	5.7×10^3	5.8×10^3	1.4×10^2	1	6.28×10^{-3}

Table 2: Impact on complexity of complexity control and projection (56 users, SNR = 12 dB).

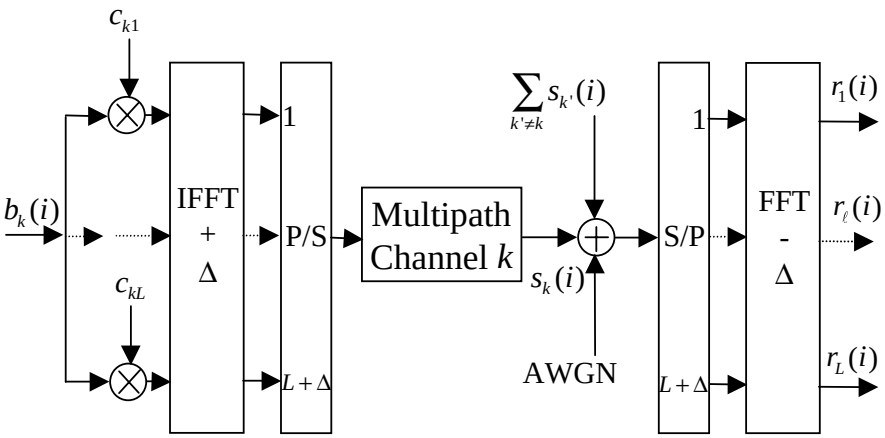

Figure 1: MC-CDMA transmitter and OFDM receiver.

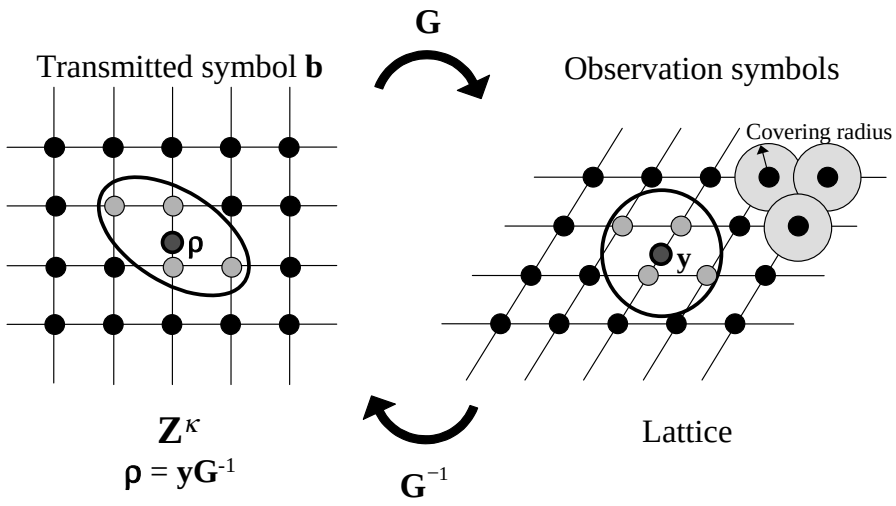

Figure 2: Geometrical representation of the sphere decoding algorithm.

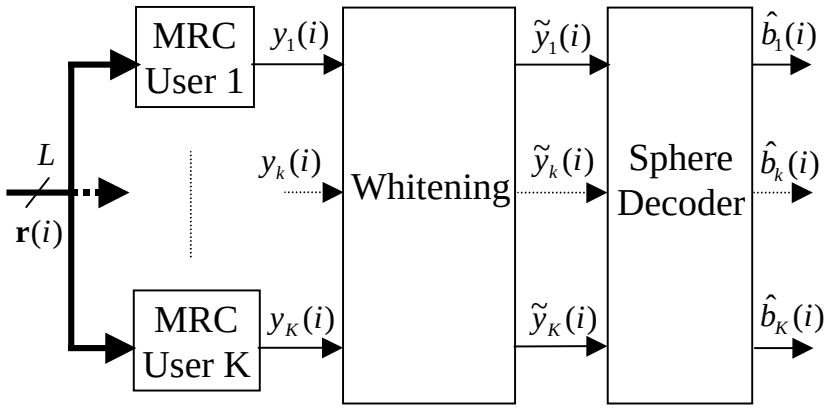

Figure 3: MC-CDMA detector with sphere decoding (after FFT).

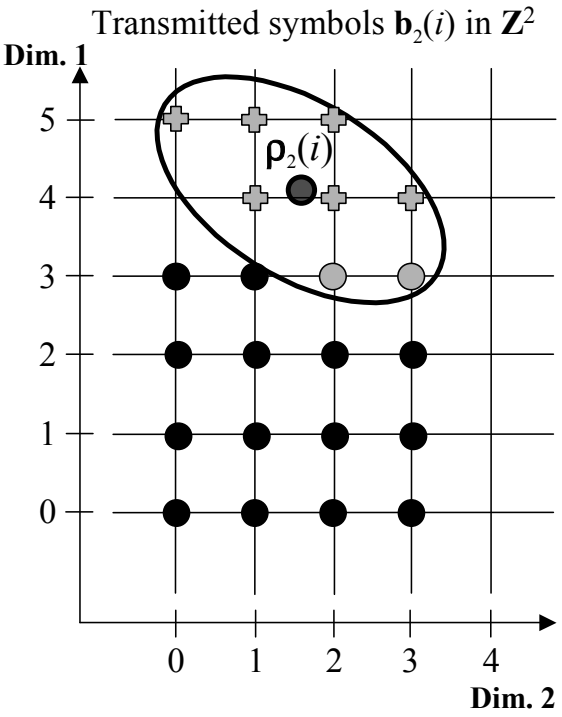

Figure 4: Sphere decoding with a finite constellation ($2K = 2$).

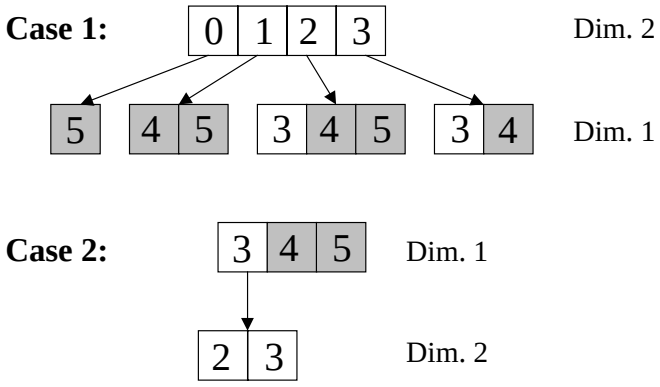

Figure 5: Optimisation of the sphere decoding search tree ($2K = 2$).

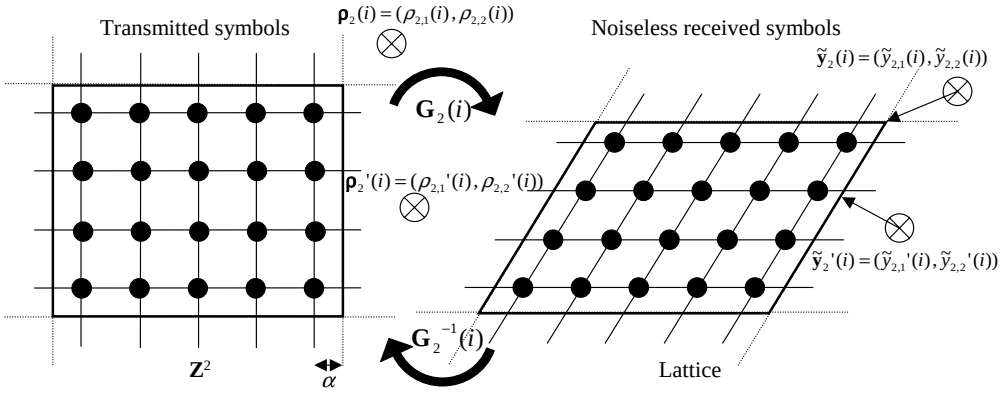

Figure 6: Determination of the projection ($2K = 2$).

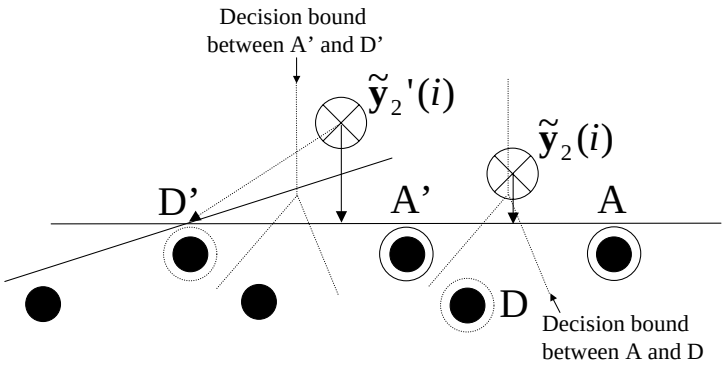

Figure 7: Projection sub-optimality ($2K = 2$).

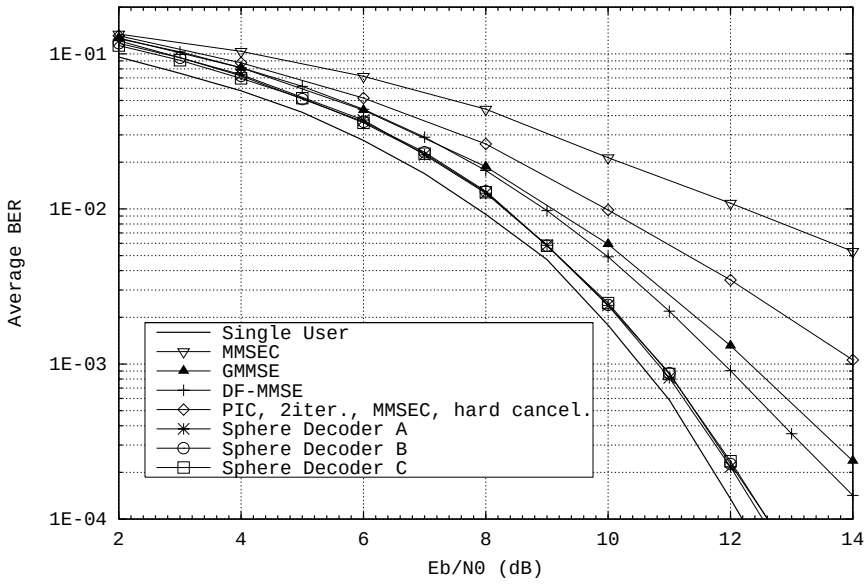

Figure 8: Comparison of various detection techniques, 32 users.

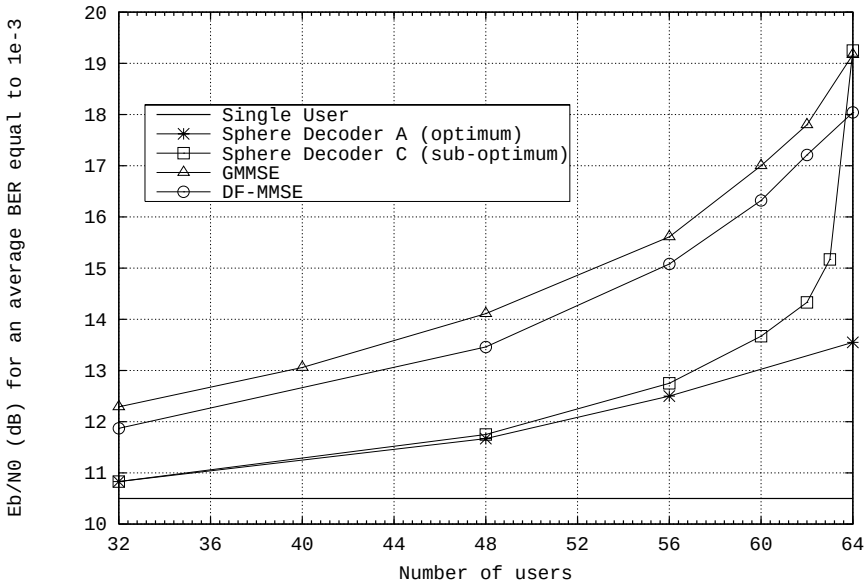

Figure 9: Comparison of various detection techniques, average BER = 10^{-3}.